J|A|C|S ARTICLES

Published on Web 04/30/2010

Unprecedented Near-Infrared (NIR) Emission in Diplatinum(III) (d^7-d^7) Complexes at Room Temperature

Martin A. Bennett,[‡] Suresh K. Bhargava,*[,†] Eddie Chung-Chin Cheng,[§] Wai Han Lam,[§] Terence Kwok-Ming Lee,[§] Steven H. Privér,[†] Jörg Wagler,[‡,#] Anthony C. Willis,[‡] and Vivian Wing-Wah Yam*[,§]

School of Applied Sciences (Applied Chemistry), RMIT University, GPO Box 2476 V, Melbourne, Victoria 3001, Australia, Research School of Chemistry, Australian National University, Canberra, ACT 0200, Australia, and Department of Chemistry, The University of Hong Kong, Pokfulam Road, Hong Kong, P.R. China

Received January 11, 2010; E-mail: suresh.bhargava@rmit.edu.au; wwyam@hku.hk

Abstract: The synthesis and single-crystal X-ray structures of the first family of efficient NIR emitters with tunable emission energy based on dihalodiplatinum(III) ($5d^7-5d^7$) complexes of general formulae $[Pt_2(\mu\text{-}C_6H_3\text{-}5\text{-}R\text{-}2\text{-}AsPh_2)_4X_2]$ (R = Me or $CHMe_2$; X = Cl, Br or I), together with that of their diplatinum(II) ($5d^8-5d^8$) precursors ($[Pt_2(\mu\text{-}C_6H_3\text{-}5\text{-}R\text{-}2\text{-}AsPh_2)_4]$) and cyano counterparts (X = CN), are reported. The diplatinum(II) complexes with isopropyl groups are isolated initially as a mixture of two species, one being a half-lantern structure containing two bridging and two chelate C_6H_3-5-$CHMe_2$-2-$AsPh_2$ ligands (**1b**) that exists in two crystalline modifications [d(Pt···Pt) = 3.4298(2) Å and 4.3843(2) Å]; the other is a full-lantern or paddle-wheel structure having four bridging C_6H_3-5-$CHMe_2$-2-$AsPh_2$ ligands (**2b**) [d(Pt···Pt) = 2.94795(12) Å]. Complete conversion of the isomers into **2b** occurs in hot toluene. The Pt−Pt bond distances in the diplatinum(III) complexes are less than that in **2b** and increase in the order X = Cl (**3b**) [2.6896(2) Å] < Br (**4b**) [2.7526(3) Å] < I (**5b**) [2.7927(7) Å] ∼ CN (**6b**) [2.7823(2), 2.7924(2) Å for two independent molecules]. Comparison with the corresponding data for our previously reported series of complexes **3a**−**6a** (R = Me) indicates that the Pt−Pt bond lengths obtained from single-crystal X-ray analysis are influenced both by the axial ligand and by intermolecular lattice effects. Like $[Pt_2(\mu\text{-pop})_4]^{4-}$ [pop = pyrophosphite, $(P_2O_5H_2)^{2-}$], the diplatinum(II) complexes $[Pt_2(\mu\text{-}C_6H_3\text{-}5\text{-}R\text{-}2\text{-}AsPh_2)_4]$ [R = Me (**2a**), $CHMe_2$ (**2b**)] display intense green phosphorescence, both as solids and in solution, and at room temperature and 77 K, with the emission maxima in the range 501−532 nm. In contrast to the reported dihalodiplatinum(III) complexes $[Pt_2(\mu\text{-pop})_4X_2]^{4-}$ that exhibit red luminescence only at 77 K in a glass or as a solid, complexes **3a**−**6a** and **3b**−**6b** are phosphorescent in the visible to near-infrared region at both room and low temperatures. The electronic spectra and photoemissive behavior are discussed on the basis of time-dependent density functional theory (TDDFT) calculations at the B3YLP level. The photoemissive states for the halide analogues **3a**,**b**−**5a**,**b** involve a moderate to extensive mixing of XMMCT character and MC [$d\sigma-d\sigma^*$] character, whereas the cyano complexes **6a** and **6b** are thought to involve relatively less mixing of the XMMCT character into the MC [$d\sigma-d\sigma^*$] state.

Introduction

Dinuclear platinum(III) complexes have been extensively studied, not only for theoretical interest but also for their potential use as catalysts and anticancer drugs.[1] However, unlike the well-studied diplatinum(II) d^8-d^8 complexes,[1b,2] the luminescence properties of the platinum(III) dimers have seldom been explored. In general, common d^7-d^7 complexes are regarded as nonemissive because their lowest-energy electronic states are extremely short-lived; the only exceptions are the $[Pt_2(\mu\text{-pop})_4X_2]^{4-}$ (pop = *P*,*P*-pyrophosphite, $P_2O_5H_2^{2-}$, X = Cl, Br, SCN or py) systems which exhibit strong red luminescence in an alcohol glass or in a solid state at low temperature.[1a,b] Apart from the $[Pt_2(\mu\text{-pop})_4X_2]^{4-}$ system, little is known of the luminescence properties of dinuclear d^7-d^7 systems. Given the promising red luminescence behavior of $[Pt_2(\mu\text{-pop})_4X_2]^{4-}$, albeit in low-temperature glass and low-temperature solid state, an exploration into dinuclear platinum(III) systems with appropriately designed rigid bridging ligands, red to near-infrared (NIR) room-temperature emissive d^7-d^7 complexes might be envisaged. In particular, NIR-emissive materials have attracted increasing attention because of their potential applications in areas such as optical communication,[3] night-vision readable displays,[4] NIR OLEDs,[5] and imaging.[6]

In the course of studies of *ortho*-metalated complexes of triarylphosphines and triarylarsines, we showed that the reaction of $[PtCl_2(SEt_2)_2]$ with 2-Li-4-$MeC_6H_3AsPh_2$ at −30 °C affords a mixture of two dinuclear complexes of platinum(II) ($5d^8-5d^8$), **1a** and **2a**,[7] of empirical formula $Pt(MeC_6H_3AsPh_2)_2$, as shown in Scheme 1.

[†] RMIT University.
[‡] Australian National University.
[§] The University of Hong Kong.
[#] Present address: Institut für Anorganische Chemie, Technische Universität Bergakademie, Freiberg D-09596, Germany.

 10.1021/ja1002313

Scheme 1

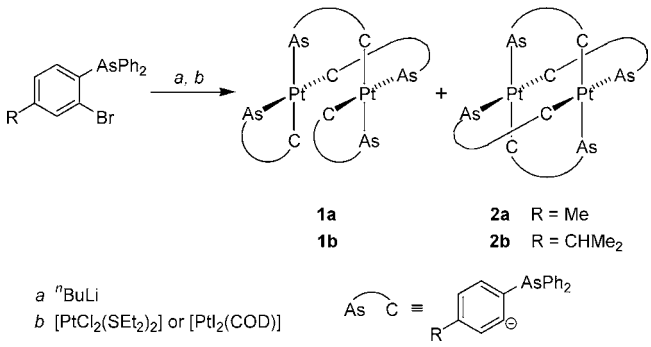

In **1a**, two of the C_6H_3-5-Me-2-$AsPh_2$ groups behave as chelate ligands while the other two bridge the metal atoms, whereas in **2a** all four C_6H_3-5-Me-2-$AsPh_2$ groups span the metal atoms to give a lantern or paddle-wheel structure. For convenience, we refer to these as half-lantern and full-lantern structures, respectively. The basic geometry of the full-lantern structure is similar to that adopted by $[Pt_2(\mu\text{-pop})_4]^{4-}$[1b] and by many other platinum(II) dimers containing S−S, N−S, and N−N donor sets.[8,9] In refluxing toluene, **1a** is converted completely into **2a**. The full-lantern structure of **2a** is retained in the metal−metal bonded dihalodiplatinum(III) ($5d^7$−$5d^7$) complexes **3a**−**5a** that are formed by oxidative addition of halogens, either to pure **2a** or to the isomeric mixture of **1a** and **2a**. The axial halides can be replaced by other anions, again without disrupting the lantern structure; for example, reaction with AgCN gives the dicyano complex **6a** (Scheme 2). Similar reactions occur in the $[Pt_2(\mu\text{-pop})_4]^{4-}$ series.[1b]

The observation that mixtures of **1a** and **2a**, and pure **2a**, show intense yellow-green luminescence in the solid state under UV-irradiation, similar to that of the much-studied salts of $[Pt_2(\mu\text{-pop})_4]^{4-}$,[1b] prompted us to examine in detail the photophysical properties of the diplatinum(II) and diplatinum(III) complexes of *ortho*-metalated tertiary arsines. To help explore the inherent photophysical properties of this class of lantern complexes, we have also prepared and studied an analogous series, the members of which bear the label b in Scheme 1, containing isopropyl in place of methyl at the 5-position of the aromatic ring. The diplatinum(III) complexes are found to exhibit intense phosphorescence in the near-infrared (NIR) region up to about 1000 nm at ambient temperature, which is a relatively rare phenomenon in transition metal complexes, and is unprecedented in diplatinum(III) systems. These properties may render the complexes promising candidates as NIR-emitting materials. The present work may open up new avenues for developing efficient NIR emitters based not only on organic compounds or metal complexes with extended π-conjugation,[5a−c,6d,10] organic donor−acceptor-/donor−acceptor−donor-type chromophores[5d,e,11] or transition metal−lanthanide complexes,[12] but also diplatinum(III) complexes with significantly short Pt−Pt distances.

Results

Synthesis. The reaction of (2-bromo-4-isopropylphenyl)diphenylarsine successively with *n*-butyl lithium and $[PtI_2(COD)]$ at 0 °C gives initially a colorless solid whose solution in dichloromethane rapidly turns yellow at or slightly above room temperature. The ^{1}H NMR spectrum of the solution contains complex, overlapping doublets in the range δ 1.07−1.23 and septets in the range δ 2.5−2.8 due to isopropyl methyl and methine protons, respectively, indicative of a mixture of species, possibly including the half-lantern (**1b**) and full-lantern (**2b**) structures. There is also a pair of closely spaced doublets of unequal intensity at δ ~7.92−7.95 with broad ^{195}Pt satellites

(1) (a) Stiegman, A. E.; Miskowski, V. M.; Gray, H. B. *J. Am. Chem. Soc.* **1986**, *108*, 2781. (b) Roundhill, D. M.; Gray, H. B.; Che, C.-M. *Acc. Chem. Res.* **1989**, *22*, 55. (c) Che, C.-M.; Butler, L. G.; Grunthaner, P. J.; Gray, H. B. *Inorg. Chem.* **1985**, *24*, 4662. (d) Che, C.-M.; Lee, W.-M.; Mak, T. C. W.; Gray, H. B. *J. Am. Chem. Soc.* **1986**, *108*, 4446. (e) Che, C.-M.; Mak, T. C. W.; Miskowski, V. M.; Gray, H. B. *J. Am. Chem. Soc.* **1986**, *108*, 7840. (f) Harvey, E. L.; Stiegman, A. E.; Week, A., Jr.; Gray, H. B. *J. Am. Chem. Soc.* **1987**, *109*, 5233. (g) Usón, R.; Forniés, J.; Falvello, L. R.; Tomás, M.; Casas, J. M.; Cotton, F. A.; Feng, X. *J. Am. Chem. Soc.* **1993**, *115*, 4145. (h) Bancroft, D. P.; Cotton, F. A.; Falvello, L. R.; Schwotzer, W. *Inorg. Chem.* **1986**, *25*, 763. (i) Bancroft, D. P.; Cotton, F. A. *Inorg. Chem.* **1988**, *27*, 4022. (j) Alonso, E.; Casas, J. M.; Cotton, F. A.; Feng, X.; Forniés, J.; Fortuño, C.; Tomás, M. *Inorg. Chem.* **1999**, *38*, 5034. (k) Woollins, J. D.; Kelly, P. F. *Coord. Chem. Rev.* **1985**, *65*, 115. (l) Appleton, T. G.; Byriel, K. A.; Hall, J. R.; Kennard, C. H. L.; Mathieson, M. T. *J. Am. Chem. Soc.* **1992**, *114*, 7305. (m) Appleton, T. G.; Byriel, K. A.; Garrett, J. M.; Hall, J. R.; Kennard, C. H. L.; Mathieson, M. T.; Stranger, R. *Inorg. Chem.* **1995**, *34*, 5646. (n) Sakai, K.; Tanaka, Y.; Tsuchiya, Y.; Hirata, K.; Tsubomura, T.; Iijima, S.; Bhattacharjee, A. *J. Am. Chem. Soc.* **1998**, *120*, 8366. (o) Lippert, B. *Coord. Chem. Rev.* **1999**, *181*, 263. (p) Cervantes, G.; Prieto, M. J.; Moreno, V. *Metal Based Drugs* **1997**, *4*, 9.

(2) (a) Fordyce, W. A.; Brummer, J. G.; Crosby, G. A. *J. Am. Chem. Soc.* **1981**, *103*, 7061. (b) King, C.; Auerbach, R. A.; Fronczek, F. R.; Roundhill, D. M. *J. Am. Chem. Soc.* **1986**, *108*, 5626. (c) Smith, D. C.; Gray, H. B. *Coord. Chem. Rev.* **1990**, *100*, 169. (d) Stiegman, A. E.; Rice, S. F.; Gray, H. B.; Miskowski, V. M. *Inorg. Chem.* **1987**, *26*, 1112. (e) Che, C.-M.; Yam, V. W.-W.; Wong, W.-T.; Lai, T.-F. *Inorg. Chem.* **1989**, *28*, 2908. (f) Yip, H.-K.; Che, C.-M.; Zhou, Z.-Y.; Mak, T. C. W. *J. Chem. Soc., Chem. Commun.* **1992**, 1369. (g) Cheung, T.-C.; Cheung, K.-K.; Peng, S.-M.; Che, C.-M. *J. Chem. Soc., Dalton Trans.* **1996**, 1645. (h) Yam, V. W.-W.; Chan, L.-P.; Lai, T.-F. *Organometallics* **1993**, *12*, 2197. (i) Yam, V. W.-W.; Yeung, P. K.-Y.; Chan, L.-P.; Kwok, W.-M.; Phillips, D. L.; Yu, K.-L.; Wong, R. W.-K.; Yan, H.; Meng, Q.-J. *Organometallics* **1998**, *17*, 2590. (j) Yam, V. W.-W.; Hui, C.-K.; Wong, K. M.-C.; Zhu, N.; Cheung, K.-K. *Organometallics* **2002**, *21*, 4326.

(3) Tessler, N.; Medvedev, V.; Kazes, M.; Kan, S.; Banin, U. *Science* **2002**, *295*, 1506.

(4) Schanze, K. S.; Reynolds, J. R.; Boncella, J. M.; Harrison, B. S.; Foley, T. J.; Bouguettaya, M.; Kang, T.-S. *Synth. Met.* **2003**, *137*, 1013.

(5) (a) Lee, T.-C.; Hung, J.-Y.; Chi, Y.; Cheng, Y.-M.; Lee, G.-H.; Chou, P.-T.; Chen, C.-C.; Chang, C.-H.; Wu, C.-C. *Adv. Funct. Mater.* **2009**, *19*, 2639. (b) Qiao, J.; Duan, L.; Tang, L.; He, L.; Wang, L.; Qiu, Y. *J. Mater. Chem.* **2009**, *19*, 6573. (c) Yan, F.; Li, W.; Chu, B.; Liu, H.; Zhang, G.; Su, Z.; Zhu, J.; Han, L.; Li, T.; Chen, Y.; Cheng, C. H.; Fan, Z. Q.; Du, G. T. *Org. Electron.* **2009**, *10*, 1408. (d) Qian, G.; Zhong, Z.; Luo, M.; Yu, D.; Zhang, Z.; Ma, D.; Wang, Z. Y. *J. Phys. Chem. C* **2009**, *113*, 1589. (e) Qian, G.; Zhong, Z.; Luo, M.; Yu, D.; Zhang, Z.; Wang, Z. Y.; Ma, D. *Adv. Mater.* **2009**, *21*, 111.

(6) (a) Werts, M. H. V.; Woudenberg, R. H.; Emmerink, P. G.; van Gassel, R.; Hofstraat, J. W.; Verhoeven, J. W. *Angew. Chem., Int. Ed.* **2000**, *39*, 4542. (b) Fragioni, J. V. *Curr. Opin. Chem. Biol.* **2003**, *7*, 626. (c) Achilefu, S. *Technol. Cancer Res. Treat.* **2004**, *3*, 393. (d) Leevy, W. M.; Gammon, S. T.; Jiang, H.; Johnson, J. R.; Maxwell, D. J.; Jackson, E. N.; Marquez, M.; Piwnica-Worms, D.; Smith, B. D. *J. Am. Chem. Soc.* **2006**, *128*, 16476.

(7) Bennett, M. A.; Bhargava, S. K.; Bond, A. M.; Edwards, A. J.; Guo, S.-X.; Privér, S. H.; Rae, A. D.; Willis, A. C. *Inorg. Chem.* **2004**, *43*, 7752.

(8) Umakoshi, K.; Sasaki, Y. *Adv. Inorg. Chem.* **1994**, *40*, 187.

(9) Cotton, F. A.; Matonic, J. H.; Murillo, C. A. *Inorg. Chem.* **1996**, *35*, 498.

(10) (a) Treadway, J. A.; Strouse, G. F.; Ruminski, R. R.; Meyer, T. J. *Inorg. Chem.* **2001**, *40*, 4508. (b) Zhang, Z.; Berezin, M. Y.; Kao, J. L. F.; Avignon, A. d'; Bai, M.; Achilefu, S. *Angew. Chem., Int. Ed.* **2008**, *47*, 3584.

(11) Riobé, F.; Grosshans, P.; Sidorenkova, H.; Geoffroy, M.; Avarvari, N. *Chem.—Eur. J.* **2009**, *15*, 380.

(12) (a) Klink, S. I.; Keizer, H.; van Veggel, F. C. J. M. *Angew. Chem., Int. Ed.* **2000**, *39*, 4319. (b) Ward, M. D. *Coord. Chem. Rev.* **2007**, *251*, 1663.

Scheme 2

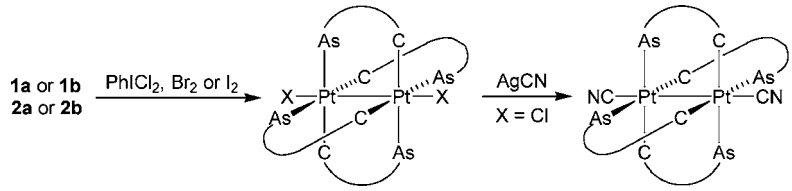

R = Me, $CHMe_2$; X = Cl (**3a**, **3b**), Br (**4a**, **4b**), I (**5a**, **5b**), CN (**6a**, **6b**)

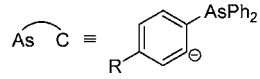

(J_{PtH} = ~59 Hz), which can be assigned to the protons *ortho* to the Pt−C bonds in **1b** and **2b**. As in the 5-methyl series, heating of the mixture in toluene causes complete conversion to the yellow-green, full-lantern dimer **2b**, which shows in its ^{1}H NMR spectrum a methyl doublet and a methine septet typical of equivalent isopropyl groups; there is also a 4H-aromatic singlet with ^{195}Pt satellites at δ 7.96 (J_{PtH} = 59.2 Hz). The ESI-mass spectrum contains an intense peak at *m*/*z* 1779 $[M + H]^+$ corresponding to the dimer.

The first formed, colorless solid may be the monomeric bis(chelate) complex [Pt(κ^2-*As*,*C*-C_6H_3-5-$CHMe_2$-2-$AsPh_2$)$_2$], analogous to the known tertiary phosphine derivative [Pt(κ^2-*P*,*C*-C_6H_3-5-R-2-PPh_2)$_2$] (R = H, Me),[13] or it may be the colorless form of the half-lantern dimer **1b** (*vide infra*). There was no evidence in the C_6H_3-5-Me-2-$AsPh_2$ series for the formation of a similar species.

Two crystals suitable for X-ray diffraction analysis were selected from the initial yellow-green solution (i.e., before heating in toluene). Both were triclinic (space group $P\bar{1}$), with similar cell dimensions, and contain the half-lantern dimer **1b**. The structures are shown with atom labeling in Figure 1 and selected molecular dimensions are listed in Table S1 (Supporting Information). Each structure contains a different conformer of the eight-membered Pt$_2$(μ-C_6H_3-5-$CHMe_2$-2-$AsPh_2$)$_2$ ring, the conformers being interconvertible by rotation about the Pt−As, Pt−C and As−Ph bonds. The main metrical difference between them lies in the intramolecular Pt···Pt separations [3.4298(1) Å, 4.3843(2) Å], the first being similar to the distances observed in the corresponding 5-methyl compound **1a** [3.4208(3) Å][7] and in the tertiary phosphine analogue [Pt$_2$(κ^2-2-$C_6H_4PPh_2$)$_2$(μ-2-$C_6H_4PPh_2$)$_2$ [3.3875(4) Å].[13] It is worth noting that the crystal of **1b** with the longer Pt···Pt distance is colorless, whereas the crystal with the shorter Pt···Pt distance is yellow. The metal−ligand bond distances and interbond angles in the conformers of **1b** do not differ significantly and show no unusual features. The bite angle in the four-membered κ^2-*As*,*C* rings is ~69°, typical of this type of compound.[14]

The full-lantern structure of complex **2b** has been confirmed by single-crystal X-ray diffraction and is shown in Figure 2 with selected molecular dimensions. The Pt···Pt separation [2.94795(12) Å] is significantly greater than that in the 5-methyl analogue **2a** [2.8955(4) Å], but both are much less than the Pt···Pt distances in the corresponding half-lantern structures.

Treatment of **2b** with $PhICl_2$ (acting as a source of Cl_2), Br_2 or I_2 gives the corresponding dihalodiplatinum(III) ($5d^7$−$5d^7$) complexes **3b**, **4b** and **5b**, as yellow-orange, brick-red and purple solids, respectively, and reaction of **3b** with AgCN gives the corresponding yellow dicyano complex **6b** (Scheme 2). X-ray crystallographic studies on single crystals of **3b**−**6b** (*vide infra*) confirm the retention of the full-lantern structure and the coordination of the anionic ligands along the Pt−Pt axis. The ESI-mass spectra show the highest mass peak at $[M - X]^+$ (X = Cl, Br, I, CN), as was observed in the 5-methyl series. In the ^{1}H NMR spectra of **3b**−**6b** the diastereotopic methyl groups on each isopropyl substituent appear as a pair of closely spaced doublets. In the precursor **2b** only one isopropyl methyl doublet

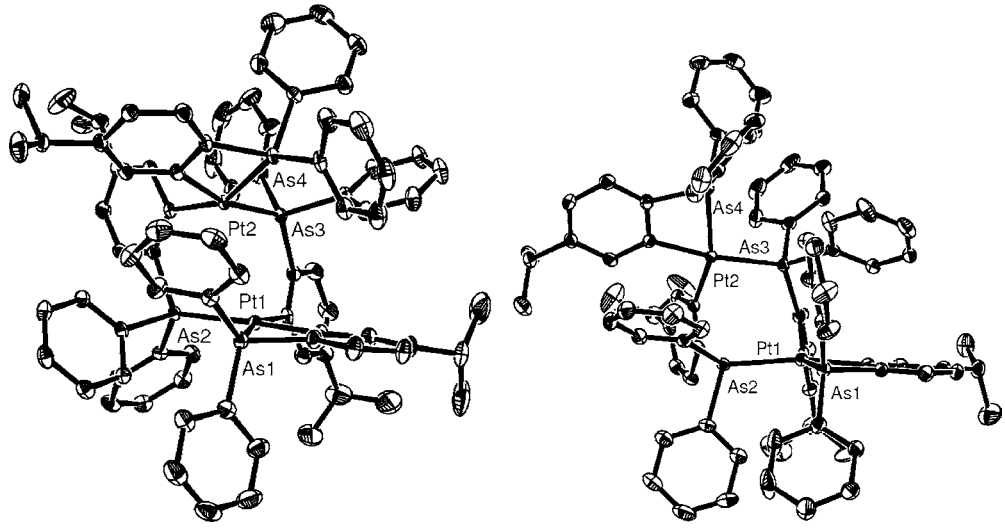

Figure 1. Molecular structures of two modifications of [Pt$_2$(κ^2-C_6H_3-5-$CHMe_2$-2-$AsPh_2$)$_2$(μ-C_6H_3-5-$CHMe_2$-2-$AsPh_2$)$_2$]·CH_2Cl_2 (**1b**) with labeling of selected atoms. Ellipsoids show 50% probability levels. Hydrogen atoms and solvent molecules have been deleted for clarity.

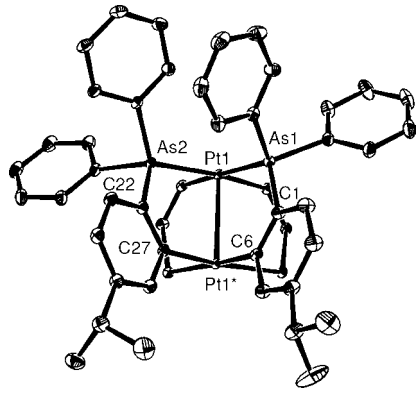

Figure 2. Molecular structure of $[Pt_2(\mu\text{-}C_6H_3\text{-}5\text{-}CHMe_2\text{-}2\text{-}AsPh_2)_4]\cdot 1.4CH_2Cl_2$ (**2b**) with labeling of selected atoms. Ellipsoids show 50% probability levels and asterisks denote atoms related by inversion symmetry. Hydrogen atoms and solvent molecules have been deleted for clarity. Two of the four C_6H_3-5-$CHMe_2$-2-$AsPh_2$ groups only show the atoms involved in the bridge framework. Selected bond lengths (Å) and angles (deg): Pt(1)−Pt(1)* 2.94795(12), Pt(1)*−C(6) 2.0545(17), Pt(1)*−C(27) 2.0629(16), Pt(1)−As(1) 2.45444(18), Pt(1)−As(2) 2.42509(17), As(1)−Pt(1)−As(2) 94.374(6), C(6)−Pt(1)*−As(1)* 176.98(5), C(27)−Pt(1)*−As(2)* 170.87(5).

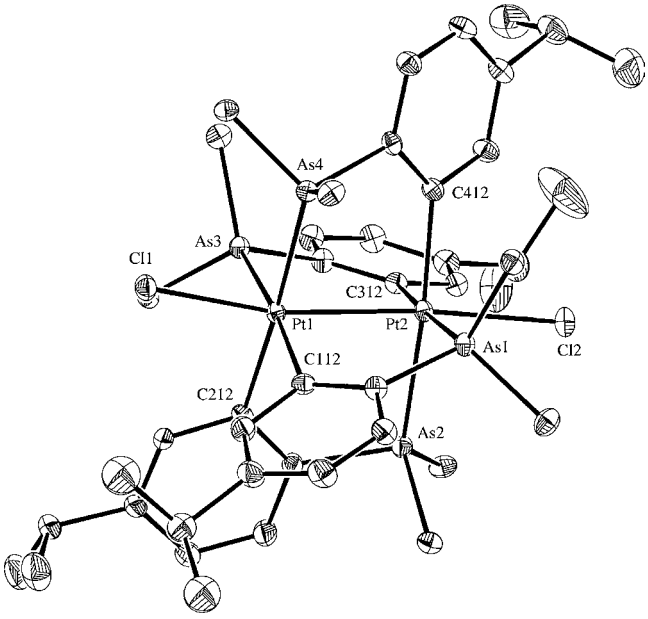

Figure 3. Molecular structure of $[Pt_2(\mu\text{-}C_6H_3\text{-}5\text{-}CHMe_2\text{-}2\text{-}AsPh_2)_4Cl_2]\cdot 2CH_2Cl_2$ (**3b**) with labeling of selected atoms. Ellipsoids show 30% probability levels. Hydrogen atoms and solvent molecules have been deleted for clarity. Only the *ipso* carbons of the $AsPh_2$ groups are shown.

is observed, possibly because the degree of inequivalence of the methyl groups is reduced by the greater separation of the metal atoms. The ^{1}H NMR spectra of **3b**−**6b** also contain the characteristic 4H-resonances at δ ~8.5, with ^{195}Pt satellites, assigned to the aromatic protons *ortho* to the Pt−C bond. The magnitude of $^3J_{PtH}$ is slightly less than those observed for the corresponding 5-methyl substituted compounds **3a**−**6a**, but, as in that series, it increases with increasing *trans*-influence of X [$^3J_{PtH}$ (Hz) = 36.6 (Cl), 38.6 (Br), 43.7 (I), 48.1 (CN)].[7]

The single-crystal X-ray structure of **3b** is shown in Figure 3. Selected bond distances and angles are collected in Tables S2 (**3b**−**5b**) and S3 (**6b**, Supporting Information). The unsolvated dibromo and diiodo complexes **4b** and **5b** (monoclinic, space group $P2_1/c$, $Z = 4$) are isomorphous and have very similar cell dimensions; the bis(dichloromethane) solvate of the dichloro complex **3b** is in the same space group with $Z = 4$ but has markedly different cell dimensions. The mono(dichloromethane) solvate of the dicyano complex **6b** is in a different space group (triclinic, space group $P\bar{1}$, $Z = 2$). By contrast, in the 5-methyl series, the dichloro-, dibromo-, and dicyano complexes, **3a**, **4a**, and **6a**, each crystallize with four dichloromethane molecules and are isomorphous with each other (triclinic, space group $P\bar{1}$, $Z = 1$), but not with the bis(dichloromethane) solvate of the diiodo complex **5a** (monoclinic, space group $P2_1/c$). We noted previously[1] that, in the 5-methyl series, the trend of increasing Pt−Pt bond distances reflects fairly well the *trans*-bond-weakening influence of the axial ligand X, i.e., 2.7444(5) Å [X = Cl (**3a**)], 2.7457(1) Å [X = Br (**4a**)], 2.752(1) Å [X = I (**5a**)] and 2.7910(2) Å [X = CN (**6a**)]. The corresponding distances in the 5-isopropyl series are 2.6986(2) Å [X = Cl (**3b**)], 2.7526(3) Å [X = Br (**4b**)], 2.7929(7) Å [X = I (**5b**)] and 2.7823(2) Å and 2.7924(2) Å (two independent molecules) [X = CN (**6b**)]. Clearly, the Pt−Pt distances for X = I and CN are almost equal, in contrast to what is found in the 5-methyl series and contrary to expectation based on *trans*-influences. Moreover, the difference in Pt−Pt distances for X = Cl and X = Br is significantly larger in the 5-isopropyl than in the 5-methyl series. Thus, the Pt−Pt distances, and to a lesser extent the Pt−X distances, are significantly affected by the change of substituent in the apparently remote 5-position as a consequence of intermolecular effects in the solid state, as well as by the electronic effects of the axial ligands.

Photophysical and Computational Studies. The photophysical properties of the platinum(II) and platinum(III) lantern dimers, and of the parent ligands 4-$RC_6H_4AsPh_2$ (R = Me, $CHMe_2$), are summarized in Table 1. The electronic absorption spectra of **2a** and **3a**−**6a** in dichloromethane at room temperature are displayed in Figure 4. The properties and trends of the methyl and isopropyl series are in general similar. The complexes exhibit high-energy absorption shoulders at 264−290 nm, which are assigned to intraligand and metal-perturbed intraligand transitions since the energies are comparable to those of the parent ligands. For the diplatinum(II) complexes **2a** and **2b**, the less intense absorption band at 406 nm is ascribed to the metal−metal-to-ligand charge transfer (MMLCT) [dσ*(Pt−Pt)→ π*(C_6H_3-5-Me-2-$AsPh_2$)] transition with the π* orbitals localized on the phenyl rings, slightly mixed with the metal-centered (MC) [dσ*→pσ] transition. Such an assignment is supported by the results obtained from TDDFT calculations (*vide infra*). Weak absorption tails, which are due to spin-forbidden ^{3}MMLCT mixed with ^{3}MC transitions, are also observed at ~460 nm (Figure 4).

The low-energy (λ > 300 nm) absorption bands of the diplatinum(III) complexes **3a**−**6a** and **3b**−**6b** occur in the region 314−512 nm (ε 9000−25000 dm^3 mol^{-1} cm^{-1}). The maxima depend strongly on the axial ligand X, with the energies decreasing in the order $X^- = CN^- > Cl^- > Br^- > I^-$, this being in line with an assignment of an axial ligand-to-metal−metal charge transfer (XMMCT) origin. TDDFT calculations indicate that these bands originate from an admixture of XMMCT transition and MC [dσ→dσ*] transitions (*vide infra*). Similar axial ligand sensitive behavior is observed for the higher in energy of the two absorptions characteristic of the diplatinu-

(13) Bennett, M. A.; Bhargava, S. K.; Messelhäuser, J.; Privér, S. H.; Welling, L. L.; Willis, A. C. *Dalton Trans.* **2007**, 3158.
(14) Mohr, F.; Privér, S. H.; Bhargava, S. K.; Bennett, M. A. *Coord. Chem. Rev.* **2006**, *250*, 1851.

Table 1. Photophysical Data for $[Pt_2(\mu\text{-}C_6H_3\text{-}5\text{-}R\text{-}2\text{-}AsPh_2)_4]$ [R = Me (**2a**), $CHMe_2$ (**2b**)], $[Pt_2(\mu\text{-}C_6H_3\text{-}5\text{-}R\text{-}2\text{-}AsPh_2)_4X_2]$ [R = Me, X = Cl (**3a**), Br (**4a**), I (**5a**), CN (**6a**); R = $CHMe_2$, X = Cl (**3b**), Br (**4b**), I (**5b**), CN (**6b**)], and $4\text{-}RC_6H_4AsPh_2$ Ligands (R = Me, $CHMe_2$)

	absorption in CH_2Cl_2 at 298 K	emission[a]	
compound	λ_{abs}/nm (ε/dm^3 mol^{-1} cm^{-1})	medium (T/K)	λ_{em}/nm (τ_o/μs)
2a	286 sh (13665), 364 (3485), 406 (7295), 462 sh (405)	solid (298)	516 (1.6)
		solid (77)	503 (2.1)
		CH_2Cl_2 (298)	532 (<0.1)
2b	290 sh (12820), 366 (3270), 406 (6615), 460 sh (395)	solid (298)	508 (1.5)
		solid (77)	501 (2.2)
		CH_2Cl_2 (298)	531 (<0.1)
3a	268 sh (43670), 290 sh (21235), 314 (16730), 414 (7290), 486 sh (2610)	solid (298)	915[b]
		solid (77)	922[b]
		CH_2Cl_2 (298)	906[b]
3b	269 sh (62610), 290 sh (32335), 312 (23045), 412 (9825), 488 sh (2910)	solid (298)	777 (4.1)
		solid (77)	778 (19.1)
		CH_2Cl_2 (298)	897 (1.3)
4a	264 sh (46770), 290 sh (19475), 334 (13505), 432 (9190) 508 sh (2850)	solid (298)	933[b]
		solid (77)	952[b]
		CH_2Cl_2 (298)	954[b]
4b	268 sh (47420), 290 sh (22395), 338 (13840), 432 sh (10780), 512 sh (2920)	solid (298)	958[b]
		solid (77)	972[b]
		CH_2Cl_2 (298)	953[b]
5a	268 sh (48280), 348 (11635), 430 (12350), 512 (24010)	solid (298)	Nonemissive
		solid (77)	1028[b]
		CH_2Cl_2 (298)	Nonemissive
5b	268 sh (44445), 348 (10540), 426 (11330), 512 (22130)	solid (298)	Nonemissive
		solid (77)	1027[b]
		CH_2Cl_2 (298)	Nonemissive
6a	260 sh (62580), 288 sh (18715), 318 (6495), 356 (9280), 444 sh (120)	solid (298)	676 (17.7)
		solid (77)	692 (29.9)
		CH_2Cl_2 (298)	726 (9.7)
6b	262 sh (60720), 290 sh (17640), 354 (8450), 442 sh (115)	solid (298)	719 (15.2)
		solid (77)	728 (29.7)
		CH_2Cl_2 (298)	719 (2.3)
$4\text{-}MeC_6H_4AsPh_2$	250 (13665), 270 sh (5170)	—[c]	—[c]
$4\text{-}Me_2CHC_6H_4AsPh_2$	250 (14540), 268 sh (6445)	—[c]	—[c]

[a] Excitation wavelength = > 300 nm. [b] Emission lifetimes in the NIR range were not measured due to the limitation of the PMT detector used for the time-resolved emission measurements. [c] Not measured.

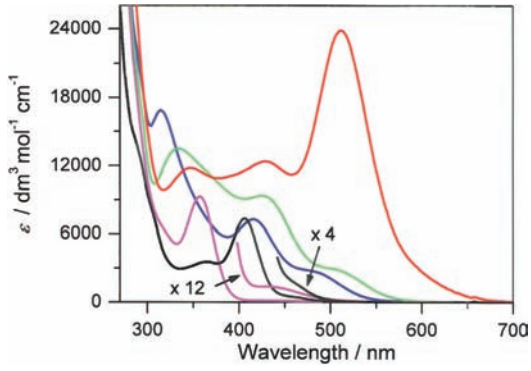

Figure 4. Electronic absorption spectra of **2a** (black) and **3a**−**6a** [X = Cl (blue), Br (green), I (red) and CN (magenta)] in dichloromethane at room temperature.

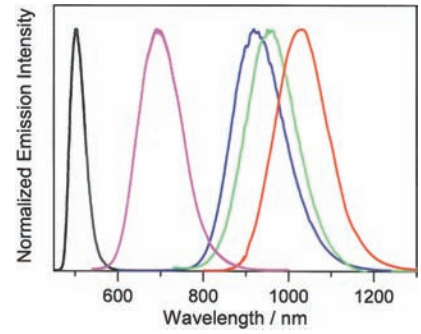

Figure 5. Emission spectra of **2a** (black) and **3a**−**6a** [X = Cl (blue), Br (green), I (red) and CN (magenta)] in the solid state at 77 K.

m(III) complexes $[Pt_2(\mu\text{-pop})_4X_2]^{4-}$.[1c] This absorption, which is ascribed to a d$\sigma\rightarrow$dσ^* transition, appears in the region 245−345 nm, and its energy decreases in the order $H_2O > Cl^- > Br^- > NO_2^- > SCN^- \sim I^-$.

Like the well-studied $5d^8$−$5d^8$ dinuclear $[Pt_2(\mu\text{-pop})_4]^{4-}$ system,[1b] the diplatinum(II) complexes **2a** and **2b** display intense phosphorescence in the range 501−532 nm, both at room temperature and 77 K, in the solid state and solution (Table 1 and Figure 5). In particular, emission maxima at 516 nm for **2a** and 508 nm for **2b** were observed in the solid state at 298 K, which can be correlated with the observed Pt···Pt distances of 2.8955(4) Å and 2.94795(12) Å, respectively. A shorter Pt···Pt distance should result in better metal-centered orbital overlaps, giving rise to larger dσ−dσ^* and pσ−pσ^* splittings, in turn reducing the dσ^*−pσ transition energy. Thus, this green phosphorescence is attributed to originate from triplet states derived from the MC [d$\sigma^*\rightarrow$pσ]/MMLCT transitions of the Pt−Pt bond.

The diplatinum(III) complexes **3a**−**6a** and **3b**−**6b** are emissive in the visible to NIR region at both room and low temperatures (Table 1 and Figures 5 and 6). This behavior differs from that of the well-studied single-bonded $5d^7$−$5d^7$ dinuclear $[Pt_2(\mu\text{-pop})_4X_2]^{4-}$ systems, which are reported to be nonemissive at ambient temperature and luminescent only at 77 K.[1b] The microsecond emission lifetimes of the diplatinum(III) complexes and large Stokes shifts indicate that the emission occurs from a triplet state. The 77 K solid-state emission energy follows the order: **5a** (1028 nm) < **4a** (952 nm) < **3a** (922 nm) < **6a** (692 nm) and **5b** (1027 nm) < **4b** (972 nm) < **3b** (778 nm) < **6b** (728 nm), which is consistent with the trends observed for the low-energy absorption band/shoulder discussed above. The emissive state for the CN analogues can be expected to have

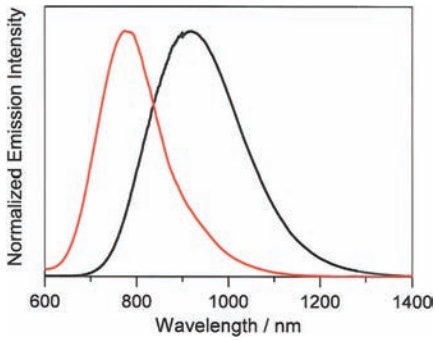

Figure 6. Emission spectra of complexes **3a** (black) and **3b** (red) in the solid state at room temperature.

relatively less mixing of the XMMCT character into the MC [dσ−dσ*] state, whereas, for the halide analogues, moderate to extensive admixture of XMMCT character with MC [dσ−dσ*] character in the emissive state, increasing from Cl to Br to I, is likely.

It is worth mentioning that one exception to the general similarity of photophysical properties of corresponding members of the 5-methyl- and 5-isopropyl-substituted series of diplatinum(III) complexes is that, in the solid state at both 298 and 77 K, the dichloro complex **3b** emits at notably higher energy (0.24−0.25 eV) than does its analogue **3a** (Table 1 and Figure 6). Even the colors of **3a** and **3b** in the solid state are visibly different (orange and golden-yellow, respectively). In contrast, the emission energies for the other corresponding members of the 5-methyl and 5-isopropyl series in the solid state differ by no more than ∼0.11 eV. This deviation must be related to the unexpectedly large difference (∼0.05 Å) in the Pt−Pt distance of **3a** and **3b** as revealed by the X-ray structural analysis; the shorter distance in **3b** would be expected to increase the dσ−dσ* energy gap and thus increase the emission energy. A similar dependence of color on Pt···Pt separation is evident in the two crystalline modifications of **1b** (*vide supra*). The assignment is further supported by the fact that the emission wavelengths of **3a** and **3b** in dichloromethane are very similar.

In order to provide a deeper understanding of the origin of the photophysical properties of the diplatinum(II) and diplatinum(III) complexes, we have carried out TDDFT calculations to compute the low-lying singlet and first triplet excited states of complexes **2a**−**6a** based on the experimental geometries obtained from the X-ray data (for details, see the Experimental Section).

For **2a**, the first two singlet−singlet transitions are calculated to be at 405 and 376 nm with oscillator strengths of $f = 0.010$ and 0.019, respectively, corresponding mainly to the excitation from the HOMO to the LUMO and LUMO+1, respectively, while the first singlet−triplet transition at 440 nm is derived from three excitations, HOMO→LUMO, HOMO→LUMO+1, and HOMO→LUMO+6. The HOMO is the Pt−Pt dσ* antibonding molecular orbital (MO), and the LUMOs are mainly the π* orbitals localized on the phenyl rings of the C_6H_3-5-Me-2-$AsPh_2$ ligand. It is worth mentioning that the π* orbitals in LUMO+1 and LUMO+6 are slightly mixed with the Pt−Pt pσ bonding MO. Therefore, the lower-energy transitions in **2a** can be assigned to MMLCT [dσ*→π*(C_6H_3-5-Me-2-$AsPh_2$)] transitions with the π* orbitals localized on the phenyl rings containing some MC [dσ*−pσ] character.

The lowest-energy singlet−singlet (dipole-allowed) and singlet−triplet transitions of the diplatinum(III) complexes **3a**−**6a** and the molecular orbitals involved in both transitions are shown in Table 2 and Figure 7, respectively. In general, both transitions in each of the diplatinum(III) complexes correspond to excitation from the Pt−Pt dσ bonding MO to the Pt−Pt dσ* antibonding MO. Table S4 (Supporting Information) shows the percentage composition and contribution of the Pt atomic orbitals to the two MOs in **3a**−**6a** (although the metal orbitals for the Pt−Pt bond involved have appreciable s and p characters in some cases, d orbitals still make the largest contribution and thus the designation dσ and dσ* would still be used for the description). As shown in Figure 7, moderate to extensive mixing from the σ donor orbital of the axial ligands X can be found in both the Pt−Pt dσ and dσ* MOs in an antibonding fashion. For the iodo complex **5a**, the Pt−Pt σ bonding MO shows a substantial mixing of the Pt−I dπ−pπ antibonding orbital which lies perpendicular to the Pt−Pt axis. The calculations indicate that the lowest energy singlet−singlet and singlet−triplet transitions contain an admixture of MC [dσ−dσ*] and XMMCT characters. The calculated energies for these transitions in the dinuclear platinum(III) complexes are in the order CN > Cl > Br > I, which is in agreement with the trend observed from the lowest-energy shoulder/band in the electronic absorption spectra.

Table 2. TDDFT Vertical Excitation Wavelength (nm) of Selected Low-Lying Singlet (S_n) and the First Triplet Excited States (T_1) in [$Pt_2(\mu$-C_6H_3-5-Me-2-$AsPh_2)_4X_2$] [X = Cl (**3a**), Br (**4a**), I (**5a**), CN (**6a**)] with the Orbitals Involved in the Excitation (H = HOMO and L = LUMO)

complex	transition	excitation[b]	*E* (nm)
3a	S_0→S_2 (0.035)[a]	H−1→L (0.56)[c]	445
	S_0→T_1 (0.000)[a]	H−1→L (0.60)[c]	525
4a	S_0→S_2 (0.032)[a]	H−1→L (0.46)[c]	463
	S_0→T_1 (0.000)[a]	H−1→L (0.71)[c]	568
5a	S_0→S_1 (0.002)[a]	H→L (0.56)[c]	560
	S_0→T_1 (0.000)[a]	H→L (0.58)[c]	688
6a	S_0→S_1 (0.095)[a]	H→L (0.64)[c]	339
	S_0→T_1 (0.000)[a]	H→L (0.71)[c]	407

[a] Oscillator strengths (*f*). [b] Excitation with the largest transition coefficient. [c] Transition coefficients.

One would expect that the Pt−Pt dσ−dσ* transition energy would be low for the dicyano complexes **6a** and **6b** because of their larger Pt−Pt separations, but this is contrary to observation. As shown in Figure 7, the energy differences between the Pt−Pt dσ and dσ* MOs are found in the order of **6a** (4.20 eV) > **3a** (3.53 eV) > **4a** (3.38 eV) > **5a** (2.94 eV), which is also in line with the calculated transition energies. The unexpected results are related to the finding that the Pt−Pt dσ bonding orbital contains Pt−X σ* antibonding character. Because the σ donor orbital localized on the carbon center of the CN ligand is the most low-lying,[15] it would be expected that the contribution from the axial ligand in the Pt−Pt dσ bonding orbital is the smallest. As a consequence, the contribution of the metal orbitals for the Pt−Pt bond would be the most significant, leading to the largest dσ−dσ* splitting and hence the largest transition energy. On the other hand, a larger contribution from the axial ligands to the Pt−Pt dσ bonding orbital is to be expected for X = halide; this increases in the order Cl < Br < I, because of the decrease in the electronegativity of the halogen. The contribution of the metal orbitals for the Pt−Pt bond decreases in the same order, leading to the decrease in the Pt−Pt dσ−dσ* splitting.

As shown in Figure 4, several absorption bands/shoulders in the lower-energy region were observed for the dihalodiplatinum(III) series. TDDFT calculations reveal that several transitions in the halide series are computed to occur at lower energies

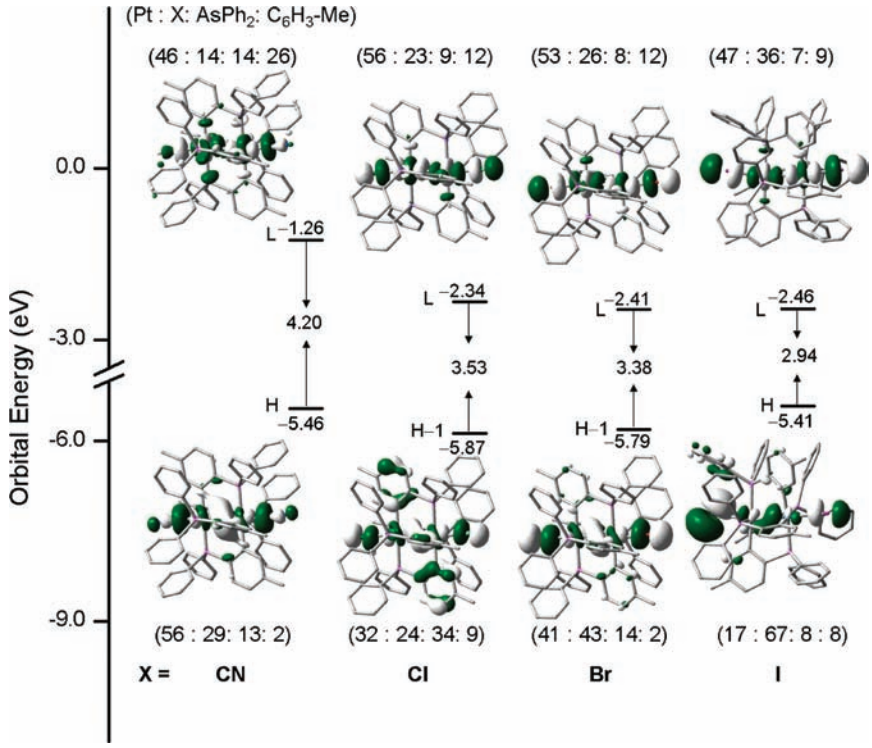

Figure 7. Energy diagram of the molecular orbitals (H = HOMO and L = LUMO) involved in the excitation shown in Table 2 with the calculated percentage compositions which are expressed in terms of contributions from the two Pt metal centers (Pt), two axial ligands (X), and diphenylarsine ($AsPh_2$) and *ortho*-metalated aryl groups (C_6H_3-5-Me) of the four bridging ligands.

than the ^{1}MC [d$\sigma\rightarrow$dσ^*]/^{1}XMMCT transition in the dicyano complex **6a**, which is calculated to occur at 339 nm. These transitions include the excitation from p orbitals of the halide ligands and π orbitals of phenyl/tolyl rings of the C_6H_3-5-Me-2-$AsPh_2$ ligands to the Pt−Pt dσ^* orbital, respectively, which can be assigned as XMMCT and ligand-to-metal−metal charge transfer (LMMCT) transitions (see Tables S5−S7, Supporting Information). For the diiodo complex **5a**, the S_2, S_3, and S_4 singlet excited states, computed to occur at 534, 522, and 518 nm, respectively, contain predominantly XMMCT character.

Conclusions

In summary, the synthesis, structures and luminescence behavior of the first family of efficient NIR emitters based on diplatinum(III) complexes and their diplatinum(II) precursors have been studied. The origin and band position of the lowest-energy absorption and emission in the diplatinum(III) complexes [$Pt_2(\mu$-C_6H_3-5-R-2-$AsPh_2)_4X_2$] (R = Me, $CHMe_2$; X = Cl, Br, I, CN) depend strongly on both the nature of the axial ligands and the Pt−Pt separation. A simple correlation of the dσ−dσ^* transition energy with the Pt−Pt bond distance in the solid state is therefore not possible. The mixing of the σ donor orbital of the axial ligands with the metal orbitals for the Pt−Pt bond has been found to show a strong influence on the dσ−dσ^* energy splitting and hence on the transition energy.

Experimental Section

General Comments. All experiments involving organolithium reagents were performed under an atmosphere of dry argon with use of standard Schlenk techniques, although the solid platinum complexes, once isolated, were air-stable. Diethyl ether, *n*-hexane, and toluene were dried over sodium and dichloromethane over calcium hydride and distilled under nitrogen prior to use. ^{1}H NMR (300 MHz) and ^{13}C NMR (75 Mz) spectra were measured on a Bruker Aspect 2000 in $CDCl_3$ or CD_2Cl_2. Chemical shifts (δ) are given in ppm, internally referenced to residual solvent signals (^{1}H: δ 5.32 for CD_2Cl_2 and δ 7.26 for $CDCl_3$; ^{13}C: δ 77.0 for $CDCl_3$); multiplicities are quoted without ^{195}Pt satellites. Elemental analyses were performed by the Microanalytical Unit at the Research School of Chemistry, Australian National University, Canberra, on samples that had been dried at 50 °C *in vacuo* to remove residual solvent. Mass spectral data were obtained on a Bruker Apex 3 and melting points were measured on a Gallenkamp melting point apparatus in open glass capillaries and are uncorrected. [PtI_2(COD)],[16] [$PdCl_2(NCMe)_2$],[17] $Me_3SiAsPh_2$,[18] $PhICl_2$[19] and the 5-methyl-substituted platinum complexes **1a**−**6a**[7] were prepared by literature methods. 3-Bromo-4-iodo(isopropyl)benzene was synthesized by the bromination of 4-isopropylaniline[20] followed by diazotization[21] as described in the literature.

Preparations: 2-Br-4-$CHMe_2$-$C_6H_3AsPh_2$. To a solution of 3-bromo-4-iodo(isopropyl)benzene (10.0 g, 0.03 mol) and [$PdCl_2(NCMe)_2$] (0.04 g, 0.15 mmol) in dry toluene (60 mL) under argon, was added $Me_3SiAsPh_2$ (9.8 g, 0.032 mol), and the dark mixture was stirred for 3 d at 80 °C. To the cooled mixture, dichloromethane (60 mL) was added, and the solution was washed

(15) DFT calculations at the B3LYP level of theory were performed on CN^- and Cl^-. The HOMO in CN^-, which is a σ donor orbital on carbon, is calculated to be lower-lying than the HOMO in Cl^-, in agreement with the higher ionization energy found in CN^-. Lloyd, D. R. *Chem. Phys. Lett.* **2000**, *323*, 198.

(16) Clark, H. C.; Manzer, L. E. *J. Organomet. Chem.* **1973**, *59*, 411.
(17) Hartley, F. R.; Murray, S. G.; McAuliffe, C. A. *Inorg. Chem.* **1979**, *18*, 1394.
(18) Fenske, D.; Teichert, H.; Poksch a, H.; Renz, W.; Becker, H. *Monatsh. Chem.* **1980**, *111*, 177.
(19) Lucas, H. J.; Kennedy, E. R. *Organic Syntheses*; John Wiley and Sons: New York, 1955; *Collect. Vol. III*, p 482.
(20) Izmer, V. V.; Lebedev, A. Y.; Nikulin, M. V.; Ryabov, A. N.; Asachenko, A. F.; Lygin, A. V.; Sorokin, D. A.; Voskoboynikov, A. Z. *Organometallics* **2006**, *25*, 1217.
(21) Boise, R.; Matzger, A. J.; Vollhardt, K. P. C. *J. Am. Chem. Soc.* **1997**, *119*, 2052.

Table 3. Crystal and Refinement Data for Complexes **1b**−**6b**

	1b[a]	**1b**[b]	**2b**	**3b**
formula	$C_{84}H_{80}As_4Pt_2 \cdot CH_2Cl_2$	$C_{84}H_{80}As_4Pt_2 \cdot CH_2Cl_2$	$C_{84}H_{80}As_4Pt_2 \cdot 1.4CH_2Cl_2$	$C_{84}H_{80}As_4Cl_2Pt_2 \cdot 2CH_2Cl_2$
fw	1864.27	1864.27	1898.24	2020.20
crystal system	triclinic	triclinic	triclinic	monoclinic
space group	$P\bar{1}$	$P\bar{1}$	$P\bar{1}$	$P2_1/c$
a, Å	12.65300(10)	12.84470(10)	12.25080(10)	19.7061(2)
b, Å	15.2413(2)	14.2111(2)	12.28270(10)	16.8389(1)
c, Å	21.8305(2)	22.2162(2)	12.7841(2)	25.4236(2)
α, deg	95.1830(10)	103.0700(10)	87.5500(10)	
β, deg	106.8150(10)	94.2820(10)	79.1420(10)	109.6409(5)
γ, deg	112.2230(10)	109.2350(10)	83.8340(10)	
V, Å^3	3634.60(8)	3680.33(8)	1877.79(4)	7945.45(11)
Z	2	2	1	4
color, habit	yellow block	colorless block	green block	orange needle
cryst dimens (mm^3)	0.44 × 0.24 × 0.16	0.16 × 0.14 × 0.12	0.27 × 0.21 × 0.16	0.45 × 0.13 × 0.11
D_{calc} (g cm^{-3})	1.703	1.682	1.679	1.689
μ (mm^{-1})	5.77	5.70	5.61	5.42
no. indep. reflns (R_{int})	21192 (0.051)	21404 (0.053)	19733 (0.043)	18121 (0.045)
no. of obsd. reflns [$I > 2\sigma(I)$]	18216	19733	17196	13331
no. params refined	848	853	457	904
R (F^2)	0.0305	0.0300	0.0258	0.024
R_w (F^2)	0.0705	0.0621	0.0634	0.068
ρ_{max}/ρ_{min} (e Å^{-3})	2.48/−2.20	1.39/−1.41	2.71/−2.25	1.70/−1.46

	4b	**5b**	**6b**
formula	$C_{84}H_{80}As_4Br_2Pt_2$	$C_{84}H_{80}As_4I_2Pt_2$	$C_{86}H_{80}As_4N_2Pt_2 \cdot CH_2Cl_2$
fw	1939.24	2033.24	1916.40
crystal system	monoclinic	monoclinic	triclinic
space group	$P2_1/c$	$P2_1/c$	$P\bar{1}$
a, Å	14.2622(2)	14.2887(5)	13.2149(1)
b, Å	21.2716(2)	21.2992(8)	13.6749(2)
c, Å	24.0645(2)	24.2678(9)	23.5355(3)
α, deg			76.3730(5)
β, deg	105.0773(6)	105.1147(17)	77.1321(6)
γ, deg			63.1672(6)
V, Å^3	7049.36(13)	7130.1(5)	3655.02(8)
Z	4	4	2
color, habit	brown needle	black block	yellow plate
cryst dimens (mm^3)	0.34 × 0.05 × 0.03	0.10 × 0.07 × 0.06	0.35 × 0.21 × 0.12
D_{calc} (g cm^{-3})	1.827	1.894	1.741
μ (mm^{-1})	7.01	6.67	5.74
no. indep. reflns (R_{int})	16159 (0.086)	12447 (0.084)	21411 (0.053)
no. of obsd. reflns [$I > 2\sigma(I)$]	9242	7783	16301
No. params refined	829	830	881
R (F^2)	0.025	0.051	0.029
R_w (F^2)	0.078	0.096	0.064
ρ_{max}/ρ_{min} (e Å^{-3})	2.38/−2.28	4.38/−4.68	1.71/−1.88

[a] Modification having d(Pt···Pt) = 3.4298(2) Å. [b] Modification having d(Pt···Pt) = 4.3843(2) Å.

with saturated sodium bicarbonate solution. The organic layer was separated and dried ($MgSO_4$), and the solvent was removed *in vacuo*. The dark oil was chromatographed on a silica gel column and eluted with 1:1 toluene/hexane. Removal of the solvent and recrystallization from hot ethanol gave the required product as white needles (9.2 g, 70%). Mp: 102−104 °C. ^{1}H NMR ($CDCl_3$): δ 1.23 (d, J_{HH} = 7.0 Hz, 6H, CH*Me*$_2$), 2.86 (sept, J_{HH} = 7.0 Hz, 1H, C*H*Me$_2$), 6.74 (d, J_{HH} = 7.9 Hz, 1H, aromatic H), 7.05 (dd, J_{HH} = 1.8, 7.9 Hz, 1H, aromatic H), 7.3−7.4 (m, 10H, aromatics), 7.44 (d, J_{HH} = 1.8 Hz, 1H, aromatic H). ^{13}C NMR ($CDCl_3$): δ 23.7, 33.6, 125.9, 128.6, 128.7, 130.1, 130.8, 133.8, 134.7, 138.3, 139.0, 151.8. ESI-MS (*m*/*z*): 426 [M]$^+$. Anal. Calcd for $C_{21}H_{20}AsBr$: C, 59.04; H, 4.72; Br, 18.70. Found: C, 59.09; H, 4.71; Br, 18.83.

4-RC$_6$H$_4$AsPh$_2$ (R = Me, CHMe$_2$). To a solution of 2-Br-4-R-C$_6$H$_3$-2-AsPh$_2$ (R = Me, CHMe$_2$) (3.0 mmol) in diethyl ether (20 mL) cooled to 0 °C was added ^{n}BuLi (1.6 M, 2.0 mL, 3.2 mmol) dropwise. After being stirred for 30 min, the solution was hydrolyzed and the organic layer was separated. The aqueous phase was extracted with diethyl ether (2 × 10 mL) and the combined organic extracts were dried ($MgSO_4$). Filtration and evaporation gave a yellow gummy solid which was recrystallized from hot ethanol to give 4-RC$_6$H$_4$AsPh$_2$ as colorless needles in yields of ∼80%.

R = Me. Mp: 49−50 °C. ^{1}H NMR ($CDCl_3$): δ 2.36 (s, 3H, Me), 7.21 (AB q, J_{HH} = 7.9, 27.7 Hz, 4H, aromatics), 7.3−7.4 (m, 10H, aromatics). ^{13}C NMR ($CDCl_3$): δ 21.3, 128.3, 128.6, 129.5, 133.6, 133.7, 135.9, 138.3, 139.9. ESI-MS (*m*/*z*): 321 [M + H]$^+$. Anal. Calcd for $C_{19}H_{17}As$: C, 71.26; H, 5.35. Found: C, 71.21; H, 5.36.

R = CHMe$_2$. Mp: 55−56 °C. ^{1}H NMR ($CDCl_3$): δ 1.27 (d, J_{HH} = 7.0 Hz, 6H, CH(*Me*)$_2$), 2.91 (sept, J_{HH} = 7.0 Hz, 1H, C*H*(Me)$_2$) 7.25 (AB q, J_{HH} = 8.1, 21.7 Hz, 4H, aromatics), 7.4−7.5 (m, 10H, aromatics). ^{13}C NMR ($CDCl_3$): δ 23.9, 33.9, 126.8, 128.3, 128.6, 133.6, 133.7, 136.3, 139.9, 149.2. ESI-MS (*m*/*z*): 349 [M + H]$^+$. Anal. Calcd for $C_{21}H_{21}As$: C, 72.41; H, 6.08. Found: C, 72.61; H, 6.10.

[Pt$_2$(κ^2-*As*,*C*-C$_6$H$_3$-5-CHMe$_2$-2-AsPh$_2$)$_2$(μ-κ*As*,κ*C*-C$_6$H$_3$-5-CHMe$_2$-2-AsPh$_2$)$_2$] (1b) and [Pt$_2$(μ-κ*As*,κ*C*-C$_6$H$_3$-5-CHMe$_2$-2-AsPh$_2$)$_4$] (2b). To a solution of (2-bromo-4-isopropylphenyl)diphenylarsine (1.09 g, 2.55 mmol) in diethyl ether (20 mL) cooled to 0 °C was added ^{n}BuLi (1.6 M, 1.6 mL, 2.56 mmol) dropwise. After

stirring for 30 min, solid [PtI_2(COD)] (0.68 g, 1.22 mmol) was added and the stirred suspension was left to slowly warm to room temperature overnight. The volume of the solvent was reduced to half under reduced pressure and the white solid was filtered off and washed with diethyl ether (5 mL). The solid was dissolved in dichloromethane, the solution was filtered to remove lithium salts, and methanol was added to the filtrate. Evaporation under reduced pressure caused a bright yellow-green solid, probably a mixture of **1b** and **2b**, to precipitate (0.55 g, 51%). This was suspended in toluene (10 mL) and refluxed under argon overnight, during which time the solid first dissolved and then reprecipitated. After cooling to room temperature, the yellow-green solid was filtered off and recrystallized from dichloromethane/methanol to give pure **2b**. Yields were essentially quantitative. ^{1}H NMR (CD_2Cl_2): δ 1.22 (d, J_{HH} = 6.9 Hz, 6H, CH*Me*$_2$), 2.72 (sept, J_{HH} = 6.9 Hz, 1H, C*H*Me$_2$), 6.4−7.1 (m, 12H, aromatics), 7.96 (d, J_{HH} = 1.7 Hz, J_{PtH} = 59.2 Hz, 1H, aromatic H *ortho* to Pt−C). ESI-MS (*m*/*z*): 1779 [M + H]$^+$. Anal. Calcd for $C_{84}H_{80}As_4Pt_2$: C, 56.70; H, 4.53. Found: C, 57.03; H, 4.62.

[Pt$_2$(μ-κ*As*,κ*C*-C$_6$H$_3$-5-CHMe$_2$-2-AsPh$_2$)$_4$X$_2$] [X = Cl (3b), Br (4b), I (5b)]. To a solution of **2b** (300 mg, 1.16 mmol) in dichloromethane (20 mL) was added one equivalent of halogen ($PhICl_2$ 47 mg; Br_2 9.7 μL; I_2 46 mg) dissolved in dichloromethane (5 mL). The yellow color immediately darkened, and the solution was stirred for 15 min. Hexane was added and the volume was reduced *in vacuo*. The precipitated solid was filtered off, washed with hexane and dried *in vacuo*.

3b: golden-yellow solid (270 mg, 87%). ^{1}H NMR (CD_2Cl_2): δ 1.22 (d, J_{HH} = 6.8 Hz, 3H, CH*Me*), 1.24 (d, J_{HH} = 7.3 Hz, 3H, CH*Me*), 2.73 (sept, J_{HH} = 6.9 Hz, 1H, C*H*Me$_2$), 6.3−7.1 (m, 12H, aromatics), 8.40 (d, J_{HH} = 1.8 Hz, J_{PtH} = 36.6 Hz, 1H, aromatic H *ortho* to Pt−C). ESI-MS (*m*/*z*): 1814 [M − Cl]$^+$. Anal. Calcd for $C_{84}H_{80}As_4Cl_2Pt_2$: C, 54.53; H, 4.36; Cl, 3.83. Found: C, 54.53; H, 4.48; Cl, 4.02.

4b: brick-red solid (276 mg, 84%). ^{1}H NMR (CD_2Cl_2): δ 1.20 (d, J_{HH} = 7.0 Hz, 3H, CH*Me*), 1.25 (d, J_{HH} = 6.8 Hz, 3H, CH*Me*), 2.70 (sept, J_{HH} = 6.9 Hz, 1H, C*H*Me$_2$), 6.3−7.1 (m, 12H, aromatics), 8.61 (d, J_{HH} = 1.5 Hz, J_{PtH} = 38.6 Hz, 1H, aromatic H *ortho* to Pt−C). ESI-MS (*m*/*z*): 1859 [M − Br]$^+$. Anal. Calcd for $C_{84}H_{80}As_4Br_2Pt_2$: C, 52.03; H, 4.16; Br, 8.24. Found: C, 52.36; H, 4.33; Br, 8.47.

5b: purple solid (310 mg, 90%). ^{1}H NMR (CD_2Cl_2): δ 1.19 (d, J_{HH} = 6.9 Hz, 3H, CH*Me*), 1.25 (d, J_{HH} = 6.8 Hz, 3H, CH*Me*), 2.67 (sept, J_{HH} = 6.9 Hz, 1H, C*H*Me$_2$), 6.2−7.1 (m, 12H, aromatics), 9.03 (d, J_{HH} = 1.8 Hz, J_{PtH} = 43.7 Hz, 1H, aromatic H *ortho* to Pt−C). ESI-MS (*m*/*z*): 1906 [M − I]$^+$. Anal. Calcd for $C_{84}H_{80}As_4I_2Pt_2$: C, 49.62; H, 3.97; I, 12.48. Found: C, 49.42; H, 4.11; I, 12.56.

[Pt$_2$(μ-κ*As*,κ*C*-C$_6$H$_3$-5-CHMe$_2$-2-AsPh$_2$)$_4$(CN)$_2$] (6b). A solution of **3b** (280 mg, 0.15 mmol) in dichloromethane was treated with an excess of AgCN (80 mg, 0.6 mmol), and the suspension was stirred for 1 h in the dark. The yellow turbid mixture was filtered through Celite, hexane was added to the filtrate, and the volume of the solution was reduced *in vacuo*. The yellow solid that precipitated was filtered off, washed with hexane, and dried (250 mg, 90%).^{1}H NMR (CD_2Cl_2): δ 1.23 (d, J_{HH} = 6.9 Hz, 3H, CH*Me*), 1.27 (d, J_{HH} = 6.9 Hz, 3H, CH*Me*), 2.76 (sept, J_{HH} = 6.8 Hz, 1H, C*H*Me$_2$), 6.3−7.1 (m, 12H, aromatics), 8.61 (s, J_{PtH} = 48.1 Hz, 1H, aromatic H *ortho* to Pt−C). ESI-MS (*m*/*z*): 1805 [M − CN]$^+$. Anal. Calcd for $C_{86}H_{80}As_4N_2Pt_2$: C, 56.40; H, 4.40; N, 1.53. Found: C, 56.48; H, 4.43; N, 1.53.

Photophysical Measurements and Instrumentation. The electronic absorption spectra were recorded on a Hewlett-Packard 8452A diode array spectrophotometer. Steady-state emission and excitation spectra recorded at room temperature and at 77 K were obtained on a Spex Fluorolog-3 model FL3-211 fluorescence spectrofluorometer equipped with a R2658P PMT detector and an In−Ga−As detector. All solutions for photophysical studies were prepared in a high-vacuum system by condensing solvent on to the solid samples contained in a 10 mL round-bottom flask equipped with a Rotaflo HP6/6 quick-release Teflon stopper. Solutions were rigorously degassed on a high-vacuum line in a two-compartment cell with no less than four successive freeze−pump−thaw cycles. Solid-state photophysical measurements were carried out with the solid sample loaded into a quartz tube inside a quartz-walled Dewar flask. Liquid nitrogen was placed in the Dewar flask for low temperature (77 K) measurements. Luminescence lifetime measurements were performed using a conventional laser system. The excitation source was the 355 nm output (third harmonic) of a Spectra-Physics Quanta-Ray Q-switched GCR-150-10 pulsed Nd:YAG laser. Luminescence decay signals from a Hamamatsu R928 PMT were converted to voltage changes by connecting to a 50 Ω load resistor and were then recorded on a Tektronix Model TDS-620A digital oscilloscope. The lifetime τ was determined by a single exponential fitting of the luminescence decay trace with the relationship $I = I_0 \exp(-t/\tau)$, where I and I_0 are the luminescence intensities at times t and 0, respectively.

Computational Details. Calculations were carried out using Gaussian 03[22] and time-dependent density functional theory (TD-DFT)[23] at the B3LYP level[24] on the basis of the crystallographically determined geometries of **2a**−**6a**. All C−H bond lengths were set at 1.09 Å. The Stuttgart effective core potentials (ECPs) and the associated valence basis set were applied to describe Pt[25] and I,[26] with an f-type polarization function for Pt and a d-type polarization for I [ζ_f(Pt) = 0.993[27] and ζ_d(I) = 0.266[28]], while the 6-31G basis set[29,30] was used for H, C, N, Cl, As, and Br with a d-type polarization function for Cl, As and Br [(ζ_d(Cl) = 0.75,[29c] ζ_d(As) = 0.273,[30] ζ_d(Br) = 0.338[30]]. Mulliken population analyses were done using MullPop.[31]

X-ray Crystallography. Crystals suitable for X-ray diffraction were obtained by layering dichloromethane solutions of the complexes with methanol. Selected crystal data and details of data collection and structure refinement are in Table 3. Crystals were coated in viscous oil and mounted on fine-drawn glass capillaries. Data were collected at 100 K (complexes **1b** and **2b**) or 200 K (complexes **3b**−**6b**) on a Nonius-Kappa CCD diffractometer using graphite-monochromated Mo Kα radiation (λ = 0.71073 Å), and were measured by COLLECT.[32] The intensities of reflections were extracted and the data were reduced by use of the computer program

(22) Frisch, M. J.; et al. *Gaussian 03*, Revision C.02; Gaussian, Inc.: Wallingford CT, 2004 (see Supporting Information for the full author list).
(23) (a) Stratmann, R. E.; Scuseria, G. E.; Frisch, M. J. *J. Chem. Phys.* **1998**, *109*, 8218. (b) Bauernschmitt, R.; Ahlrichs, R. *Chem. Phys. Lett.* **1996**, *256*, 454. (c) Casida, M. E.; Jamorski, C.; Casida, K. C.; Salahub, D. R. *J. Chem. Phys.* **1998**, *108*, 4439.
(24) (a) Lee, C.; Yang, W.; Parr, P. G. *Phys. Rev. B* **1988**, *37*, 785. (b) Becke, A. D. *J. Chem. Phys.* **1993**, *98*, 5648. (c) Stephens, P. J.; Devlin, F. J.; Chabalowski, C. F.; Frisch, M. J. *J. Phys. Chem.* **1994**, *98*, 11623.
(25) Andrae, D.; Häussermann, U.; Dolg, M.; Stoll, H.; Preuss, H. *Theor. Chim. Acta* **1990**, *77*, 123.
(26) (a) Bergner, A.; Dolg, M.; Küchle, W.; Stoll, H.; Preuss, H. *Mol. Phys.* **1993**, *80*, 1431. (b) Glukhovtsev, M. N.; Pross, A.; McGrath, M. P.; Radom, L. *J. Chem. Phys.* **1995**, *103*, 1878. Erratum: *J. Chem. Phys.* **1996**, *104*, 3407.
(27) Ehlers, A. W.; Böhme, M.; Dapprich, S.; Gobbi, A.; Höllwarth, A.; Jonas, V.; Köhler, K. F.; Stegmann, R.; Veldkamp, A.; Frenking, G. *Chem. Phys. Lett.* **1993**, *208*, 111.
(28) Huzinaga, S.; Andzelm, J.; Klobukowski, M.; Radzio-Andzelm, E.; Sakai, Y.; Tatesaki, H. *Gaussian Basis Sets for Molecular Calculations*; Elsevier: Amsterdam, 1984.
(29) (a) Ditchfield, R.; Hehre, W. J.; Pople, J. A. *J. Chem. Phys.* **1971**, *54*, 724. (b) Hehre, W. J.; Ditchfield, R.; Pople, J. A. *J. Chem. Phys.* **1972**, *56*, 2257. (c) Francl, M. M.; Pietro, W. J.; Hehre, W. J.; Binkley, J. S.; Gordon, M. S.; Defrees, D. J.; Pople, J. A. *J. Chem. Phys.* **1982**, *77*, 3654.
(30) Binning, R. C., Jr.; Curtiss, L. A. *J. Comput. Chem.* **1990**, *11*, 1206.
(31) Pis Diez R. *MullPop*; National University of La Plata: Argentina.
(32) *COLLECT Software*; Nonius-BV: Delft, The Netherlands, 1997−2001.

Denzo and Scalepack.[33] The crystal structures were solved by direct methods[34] and refined on F^2 by use of either the SHELX program[35] for **1b** and **2b** or of CRYSTALS[36] for **3b**−**6b**. Neutral atom scattering factors,[37] the values of $\Delta f'$ and $\Delta f''$, and mass attenuation coefficients were taken from standard compilations.[38]

The crystallographic data have been deposited with the Cambridge Crystallographic Data Centre [CCDC 752812 (**3b**), 752813 (**4b**), 752814 (**5b**), 752815 (**6b**), 752816 (**1b**, mod 1), 752817 (**2b**) and 752818 (**1b** mod 2)].

Acknowledgment. V.W.-W.Y. acknowledges support from The University of Hong Kong under the Distinguished Research Achievement Award Scheme. W.H.L. acknowledges the receipt of a University Postdoctoral Fellowship and T.K.-M.L. the receipt of a postgraduate studentship, both from The University of Hong Kong. J.W. acknowledges the award of a postdoctoral fellowship by the German Academic Exchange Service (DAAD). This work has been supported by a GRF grant from the Research Grants Council of Hong Kong Special Administrative Region, China (HKU 7050/08P). We also thank the Computer Center at The University of Hong Kong for providing the computational resources.

Supporting Information Available: X-ray crystallographic data in CIF format for complexes **1b**−**6b**, Tables S1−S3 containing selected bond lengths and angles for complexes **1b** and **3b**−**6b**, Table S4 containing percentage contribution of Pt atomic orbitals for complexes **3a**−**6a**, Tables S5−S7 containing singlet−singlet transitions for complexes **3a**−**5a** and complete ref 22. This material is available free of charge via the Internet at http://pubs.acs.org.

JA1002313

(33) Otwinowski, Z.; Minor, W., Jr. In *Methods in Enzymology*; Carter C. W., Sweet, R. M., Eds; Academic Press: New York, 1997; Vol. 276, pp 307−326.
(34) Altomare, A.; Cascarano, G.; Giacovazzo, G.; Guagliardi, A.; Burla, M. C.; Polidori, G.; Camalli, M. *J. Appl. Crystallogr.* **1994**, *27*, 435.
(35) Sheldrick, G. M. *SHELXL-97*; University of Göttingen: Germany, 1997.
(36) Betteridge, P. W.; Carruthers, J. R.; Cooper, R. J.; Prout, K.; Watkin, D. J. *J. Appl. Crystallogr.* **2003**, *36*, 1487.
(37) *International Tables for X-ray Crystallography*; Kynoch Press; Birmingham, England, 1974; Vol. IV.
(38) *International Tables for X-ray Crystallography*; Kluwer Academic: Boston, MA, 1992; Vol. C.